PHOTONICS Research

Alloyed Au-Ag nanorods with desired plasmonic properties and stability in harsh environments

Yuan Ni,[1] Caixia Kan,[1,2,5] Longbing He,[3,4,6] Xingzhong Zhu,[1] Mingming Jiang,[1] and Daning Shi[1]

[1]College of Science, Nanjing University of Aeronautics and Astronautics, Nanjing 210016, China
[2]Key Laboratory for Intelligent Nano Materials and Devices of the Ministry of Education, Nanjing 210016, China
[3]SEU-FEI Nano-Pico Center, Key Laboratory of MEMS of the Ministry of Education, Southeast University, Nanjing 210096, China
[4]Southeast University-Monash University Joint Research Institute, Suzhou 215123, China
[5]e-mail: cxkan@nuaa.edu.cn
[6]e-mail: helongbing@seu.edu.cn

Received 11 December 2018; revised 14 February 2019; accepted 10 March 2019; posted 11 March 2019 (Doc. ID 354455); published 29 April 2019

Bio-chemical molecular detection in the nanoscale, based on alloyed nanorods (NRs) with tunable surface plasmon resonance (SPR) properties and high chemical stability, has attracted particular interest. In this work, alloyed Au-Ag NRs with tunable aspect ratios were achieved by annealing Au nanobipyramid-directed Au@Ag core-shell NRs. The core-shell NRs were encapsulated within mesoporous silica outer shells to avoid fusion or aggregation. The structural stability of fully alloyed Au-Ag NRs, including chemical and thermal stability, is remarkably improved compared with that of Au@Ag core-shell NRs. The alloyed NRs would maintain the rod-like structure after being incubated in etchant solution, while Au@Ag core-shell NRs would decay into nanobipyramids. Additionally, fully alloyed NRs present stable morphology under annealing at high temperatures of up to 600°C in air. Benefiting from excellent structural and chemical stabilities, the surface-enhanced Raman scattering effect based on alloyed NRs is stable in harsh environments. Taking advantage of tunable SPR properties (600–1800 nm) and excellent stability, the obtained nanostructures can serve as drug carriers. The perfect photo-thermal effect induced by the particular SPR of alloyed NRs can improve the release efficiency of drugs.

https://doi.org/10.1364/PRJ.7.000558

1. INTRODUCTION

Noble metal nanoparticles have been extensively investigated to apply plasmonic responses [1], upon coupling with an electromagnetic field, to many promising applications, such as photoelectronic devices [2,3], bio-medicine [4–6], and catalysis [7,8]. The plasmonic properties of metal nanoparticles are dependent on the shape, size, composition, and surrounding medium. Compared with spherical metal nanoparticles (NPs), anisotropic metal nanorods (NRs) exhibit two anisotropic surface plasmon resonance (SPR) modes, transverse SPR (SPR_T) and longitudinal SPR (SPR_L) [9–12]. Both longitudinal and transverse modes are tunable, but if the nano-rod shape is kept (i.e., one radius at least 1.5 times bigger than the other) the transverse mode is tunable in a smaller spectral range. With the increasing aspect ratio of NRs, the SPR_L can be tuned from the visible to the near-infrared (Vis-NIR) region. Systematic exploration on Au and Ag nanoparticles has been widely reported [13–15]. Although Au nanocrystals offer excellent chemical stability and tunable SPR in a large region (>500 nm), their practical applications are limited for their relatively weak surface-enhanced Raman scattering (SERS) and catalytic effects compared with similar Ag nanoparticles [16]. The plasmonic resonance in silver nanoparticles is indeed more efficient since silver has lower losses compared to gold. However, the poor chemical and structural stability of Ag impedes the fundamental research and technical applications. Moreover, the dispersity of nanoparticle colloid stabilized by surfactants is critical for application in a liquid environment. Notably, surfactants will lead to bio-toxicity and reduced adsorption between the analyte and metal core. For the case of stability and plasmonic activity, Au-Ag alloyed nanostructures provide an alternative approach by changing the alloy composition [17,18], and the advantages of mesoporous silica can be taken to avoid the bio-toxicity and provide adsorption channels.

Studies on anisotropic NRs with the advantages of alloyed materials have been reported. However, previous studies were mainly focused on the spherical Au-Ag alloyed nanoparticles, which combined both the superior properties of high chemical stability of Au nanocrystals and excellent plasmonic properties of Ag nanocrystals. Yin and co-workers have used functionalized alloyed Au-Ag nanospheres as SERS sensors for quantitative detection of endonuclease [19]. Moreover, it is reported that Au-Ag alloyed NPs can be used as stimuli for enhancing optical and mass spectrometric imaging of latent fingerprints due to the enhanced optical absorption efficiency and improved

stability [20,21]. Additionally, alloyed nanostructures also show a more active ability toward catalyzing a wider variety of reactions than pure Au or pure Ag nanoparticles [22].

Alloyed Au-Ag nanostructures were usually fabricated by laser ablation [23], solvothermal synthesis [24], co-reduction of Au and Ag salts [25], or replacement reactions [26–28]. Annealing is also an alternative approach to prepare alloyed nanostructures [29,30]. Unfortunately, annealing at a high temperature would fuse anisotropic nanostructures into nanospheres. There are only a few reports on the synthesis of fully alloyed Au-Ag NRs. Han *et al.* [31] fabricated homogeneously alloyed Au-Ag shells on Au NRs by a co-reduction method, and the SPR_L wavelength could only be tuned in a region of 648–736 nm. Although phase segregation was inevitable due to the close lattice parameters of Au (4.08 Å, 1 Å = 0.1 nm) and Ag (4.09 Å), a considerable discrepancy of surface energy between Au (97 meV/Å^2) and Ag (78 meV/Å^2) would possibly lead to the aggregation of Ag atoms on the surface of Au, forming core-shell structures rather than alloyed nanostructures [32]. Recent results show that Au-Ag alloyed NRs can be obtained by thermal treatment of Au@Ag core-shell NRs coated by mesoporous SiO_2 shells [33,34]. Notably, the deposition of Ag on transverse side surfaces of single-crystalline Au NRs is faster than in the longitudinal ending directions, and these finally result in the formation of cubic Au@Ag nanostructures [35]. The SPR_L of the resultant alloyed nanostructures could be adjusted from ~600 to ~800 nm in wavelength. Therefore, fabrication of alloyed Au-Ag NRs with highly tunable plasmonic properties is still challenging.

Herein, alloyed Au-Ag NRs with tunable aspect ratios were synthesized by annealing well-defined Au@Ag core-shell NRs with the aid of mesoporous silica. Silica capping formations on alloyed NRs are selective for carrier gas conditions. For example, annealing in air leads to hollow silica capping due to the sublimation of Ag. The SPR_L mode of alloyed NRs can be controlled from the visible to near-infrared region (600–1800 nm) by increasing the amount of $AgNO_3$. The SPR_T modes can be tuned in the spectral region of 400–500 nm by adjusting the Ag/Au composition. To investigate the chemical stability, NRs including core-shell and alloyed types are incubated in etchant (including NH_4OH and H_2O_2) solutions. Alloyed Au-Ag NRs are highly stable, while core-shell NRs transform into Au nanobipyramids (NBPs). Moreover, the thermal stability also was explored by annealing alloyed Au-Ag NRs and core-shell NRs at 600°C. Based on the excellent structural stability, the application research into alloyed NRs in the biomedical field, taking the SERS signal detection of R6G and the drugs' release as examples, was explored. It can be found that hollow silica capping can provide much more space to store the drugs. Owing to the selective photo-thermal effect based on the tunable SPR properties, the release efficiency of drugs absorbed on alloyed Au-Ag NRs will be increased. As a result, alloyed NRs are also promising candidates for bio-medicine applications.

2. EXPERIMENTAL SECTION

A. Synthesis of Au Nanobipyramids

A seed-mediated method was used to fabricate well-defined Au NBPs as reported previously [35–38]. The seed solution was prepared by adding a fresh ice-cold $NaBH_4$ solution (0.1 M, 0.2 mL; 1 M = 1 mol/L) into a mixed solution of $HAuCl_4$ (0.01 M, 0.2 mL), trisodium citrate, and deionized water under vigorous stirring. The resultant seed solution was kept at 85°C for 1.5 h to promote the formation of five-fold twined crystals. The growth solution was made by sequential addition of $HAuCl_4$ (0.05 M, 1 mL), $AgNO_3$ (0.02 M, 0.5 mL), HCl (1 M, 2 mL), and ascorbic acid (0.1 M, 0.8 mL), and the as-prepared seed solution was put into a hexadecyl trimethyl ammonium bromide (CTAB) solution (0.1 M, 100 mL) under gentle stirring for 10 s. The reaction solution was undisturbed at room temperature for 2 h to generate Au NBPs.

Typically, high-yield Au NBPs were achieved by two steps, including Ag overgrowth based on as-grown Au NBPs and the undisturbed storage and re-etching with NH_4OH (8 mL) and H_2O_2 (6%, 5 mL) solution.

B. Synthesis of Au@Ag Core-Shell NRs

Well-defined Au NBPs (90 mL) of different sizes were redispersed in a CTAB solution (0.08 M), which was followed by adding $AgNO_3$ (4–9 mL, 0.02 M) and the same amount ascorbic acid (0.1 M) to grow Au@Ag core-shell NRs with tunable aspect ratios. The Au@Ag core-shell NRs were centrifuged twice at 5300 r/min for 10 min, removing the redundant surfactant. The precipitate was dispersed in a CTAB solution (1 mM).

C. Synthesis of Au@Ag@SiO_2 Core-Shell NRs

The as-prepared Au@Ag core-shell NRs (90 mL) with the presence of CTAB were added in the mixture of NaOH (900 μL, 0.1 M) and tetraethylortho silicate (TEOS) (900 μL, 10% in ethanol) under stirring at room temperature for 20 h, during which the mesoporous silica outer shell formed through surface coating. The products were centrifuged at 5000 r/min for 8 min and then dispersed in ethanol.

D. Synthesis of Alloyed Au-Ag NRs

In situ synthesis: The alloying process is performed and observed using an *in-situ* scanning transmission electron microscope (STEM) during heating the as-prepared Au@Ag core-shell NRs on an e-chip (the vacuum level is to 4×10^{-5} Pa). The critical temperature at which alloying happened can be read out directly according to the heating setup.

Ex situ synthesis: Different aspect ratios of Au@Ag@SiO_2 core-shell NRs were placed on the quartz substrate. The dried samples were transferred to the tube furnace and flushed with N_2 for 30 min at room temperature. Subsequently, the oven was heated to 400°C with a rate of 5°C/min, kept at 400°C for 10 min and naturally cooled to room temperature in N_2 flow or air. The annealed samples could be re-dispersed in deionized water containing CTAB (0.01 M), diethylamine, and NaOH to remove the silica shell. Finally, the samples with and without silica capping were collected by centrifugation and redispersed in water for further application and characterization.

E. Characterization

Transmission electron microscopic images were taken with transmission electron microscopy (TEM, JEOL-100CX, Japan) and high-resolution TEM (FEI Tecnai 20, FEI Titan 80-300). High-angle annular dark field scanning transmission electron microscopy (HAADF-STEM), energy-dispersive X-ray

(EDX) spectra, and element mappings were measured by TecnaiG2 F20. UV-vis-NIR absorption spectra were recorded using 3600-Plus spectrophotometer. SERS spectra were acquired by Raman microscope (Finder One, Zolix, China).

F. SERS Measurements

As-prepared alloyed Au-Ag NRs and Au@Ag core-shell NRs were each incubated with rhodamine-6G (10^{-5} mol/L) overnight, and subsequently dried under N_2 flow. SERS spectra were recorded under irradiation with a 532 nm laser using an exposure of 3 s.

G. Doxorubicin Loading and Release

Alloyed Au-Ag NRs coated by mesoporous silica were mixed with doxorubicin (DOX) aqueous solution (1 mL, 1 mg/mL). The mixture was stirred at 30°C for 24 h to reach a loading equilibrium state. Subsequently, the DOX-loaded alloyed NRs were centrifuged and dispersed in phosphate buffer solution (PBS), and the supernatant was collected and measured using 3600-Plus spectrophotometer. A resonance wavelength of 480 nm (the characteristic peak of DOX) was used to estimate the amount of DOX loading. At a certain time interval, the DOX-loaded samples with and without irradiation of 980 nm laser (7.5 W/cm^2, GKD-30FMS) were centrifuged, and the supernatant was measured via the spectrophotometer. Meanwhile, fresh PBS was added for further measurements.

3. RESULTS AND DISCUSSION

A. Alloyed Au-Ag NRs with Tunable SPR Properties

A typical synthetic procedure of alloyed Au-Ag NRs is shown in Fig. 1(a). Au@Ag core-shell NRs were first prepared by overgrowing Ag on the Au NBPs. The Au@Ag core-shell NRs were subsequently coated with mesoporous silica. The core and shell parts of the NRs can be distinguished clearly from the HAADF-STEM images due to the different Z-contrast between Au and Ag, as shown in Fig. 1(b). In the process of *in situ* heating, the interface between Au and Ag vanishes momentarily at ~350°C [Fig. 1(c)], indicating the accomplishment of alloying between Au and Ag. Under the instruction of *in situ* observations, *ex situ* thermal treatments of Au@Ag@SiO_2 NRs are carried out in a furnace tube under different annealing temperatures and atmospheres to further investigate the alloying process. It has been found that Au@Ag core-shell NRs present an absorption shoulders at ~340 nm, which corresponds to the characteristic peak of anisotropic Ag NRs [Fig. 2(a)]. As the annealing temperature rises up to 400°C, SPR_T at ~400 nm presents an obvious redshift. Meanwhile, the absorption shoulder gradually decays and vanishes during increasing temperature, owing to the structural change [Fig. 2(b)].

In contrast to the heteroepitaxy growth of Ag on single-crystalline Au NRs, the growth of Ag on twined Au NBPs generally occurs along the longitudinal directions [9]. With the addition of $AgNO_3$, the high aspect ratio of Au@Ag core-shell NRs could be prepared. The tunable SPR and corresponding TEM images of the annealed precursor NRs (Au@Ag core-shell capsuled in mesoporous silica) are illustrated in Fig. 2. It can be demonstrated that the SPR_L wavelength is controllable in a large region through the change in the aspect ratio. As a result, alloyed Au-Ag NRs with highly tunable SPR can be generated by annealing the as-prepared core-shell NRs. Figures 2(b) and 2(c) reveal the spectral evolution of alloyed Au-Ag NRs as a function of the volume of $AgNO_3$ precursors, wherein the annealed samples were immersed into NaOH solution to remove the silica shells. Similar to the core-shell NRs, the SPR_L modes of alloyed NRs also present a redshift trend in the Vis-NIR region with the increasing $AgNO_3$ volume. Notably, the SPR_T modes of alloyed NRs blueshift subsequently, which is different from those of the core-shell ones. It is well known that the SPR_T modes of core-shell NRs have little shift. Increasing the addition of $AgNO_3$ would cause an increase of the Ag/Au composition ratio, which influences the structural dielectric constants [18]. Consequently, the SPR_T wavelength of alloyed Au-Ag NRs can be tuned. Corresponding to the absorption spectra, Figs. 2(d)–2(i) illustrate the TEM images of alloyed Au-Ag NRs with different aspect ratios. It is obvious that the morphology has not transformed after annealing the core-shell NRs coated by mesoporous silica.

Moreover, the elemental distribution of alloyed Au-Ag NRs (annealing at 400°C) with different aspect ratios was investigated by EDX mapping. For short alloyed Au-Ag NRs ($n = 3$), the homogeneous distribution of Au and Ag elements confirms fully alloyed structures, as shown in Fig. 2(j). In contrast, the distribution of Au atoms in NRs with high aspect ratios ($n = 6$) is inhomogeneous. Au atoms do not gradually disperse out from core; rather, they distribute at the surface of ends, forming partially alloyed Au-Ag NRs [Fig. 2(k)].

To the best of our acknowledge, the formation energy (or phase stability) of alloyed nanostructures is lower than that of core-shell nanostructures [32]. The driving force in the kinetic alloying process derives from the formation energy difference between alloy and core-shell nanostructures, which gradually decreases with diffusion of Au and Ag atoms. If the driving force (formation energy) and external effect (annealing temperature:

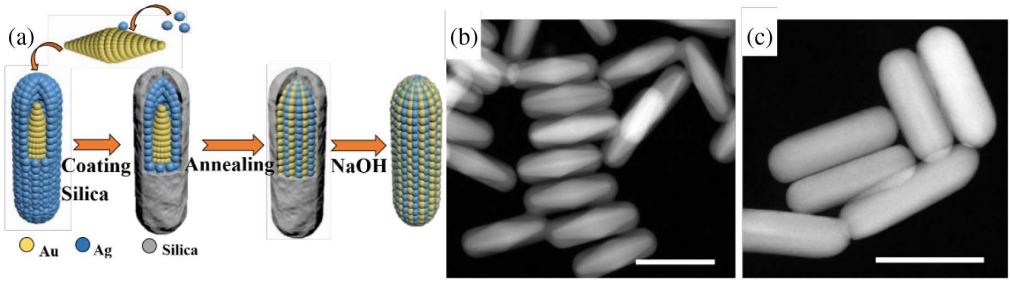

Fig. 1. (a) Schematic illustration of the synthetic process of alloyed Au-Ag NRs. HAADF-STEM images of as-prepared. (b) Au@Ag core-shell NRs and (c) alloyed NRs with *in situ* STEM heating up to 350°C (scale bars: 100 nm).

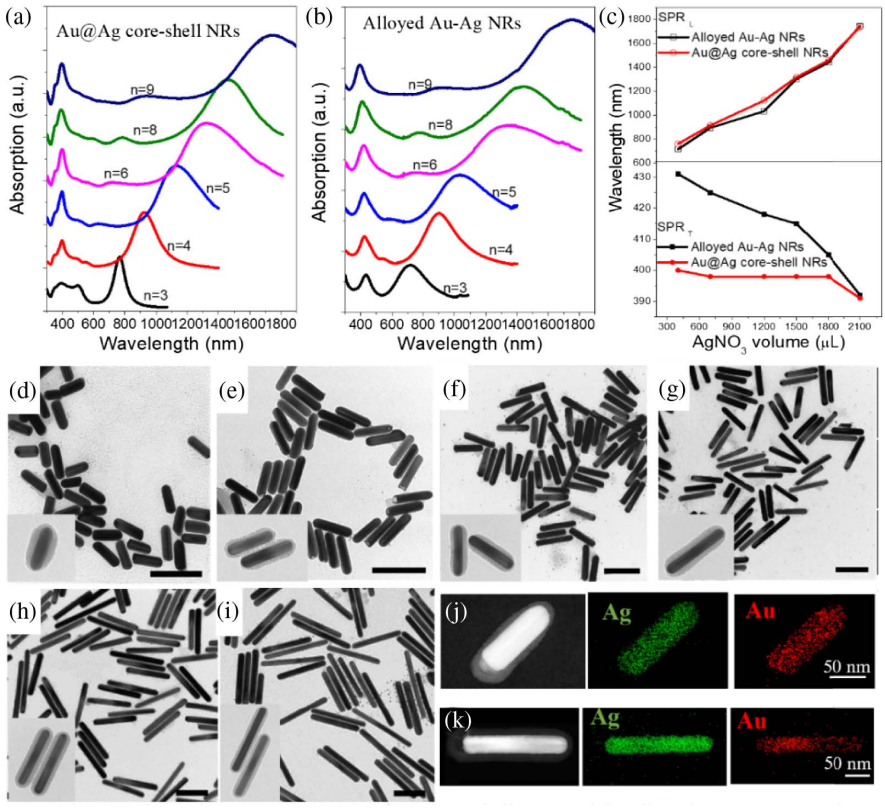

Fig. 2. UV-vis-NIR absorption spectra of (a) Au@Ag core-shell NRs and (b) alloyed Au-Ag NRs under annealing at 400°C in N_2 flow. (c) SPR_L and SPR_T wavelength versus the volume of the $AgNO_3$ precursor. (d)–(i) TEM images of alloyed Au-Ag NRs with increasing aspect ratios ($n = L/W$, the ratio between length and width of NRs, i.e., 3, 4, 5, 6, 8, 9). The insets of (d)–(i) are corresponding TEM images of Au@Ag core-shell NRs capsuled within mesoporous silica. (j),(k) HAADF-STEM images and element mapping of alloyed Au-Ag NRs (aspect ratio $n = 3$ and 6, respectively) (scale bars: 200 nm).

400°C) are not enough to reach the thermodynamic equilibrium, the final products will be surface-alloyed instead of fully alloyed.

As previously reported, the atomic diffusion (D) is dependent on the temperature, and the relation can be expressed by the Boltzmann–Arrhenius equation [24]

$$D = D_0 \exp\left(-\frac{\Delta H_d}{kT}\right), \tag{1}$$

wherein k is the Boltzmann constant, ΔH_d is the activation enthalpy of diffusion, and D_0 is the pre-exponential factor. It can be obtained that the diffusivity of atoms is accelerated exponentially with increasing annealing temperature. Therefore, higher annealing temperature can enhance the diffusion, leading to thermodynamic equilibrium. A series of annealing conditions were performed to obtain fully alloyed Au-Ag NRs. Figure 3(a) shows the absorption spectra of alloyed Au-Ag NRs under different annealing temperatures. The SPR_L and SPR_T modes have no obvious change as the annealing temperature increases to 450°C. Further raising the annealing temperature, a slight blueshift SPR_L mode appears, while the SPR_T wavelength has no change. It can be proposed that high temperature may induce slight damping of the aspect ratio of NRs. The transform of composition from partial to full alloying with increasing temperature seems to be contradictory with the unchanged SPR mode. The phenomenon is

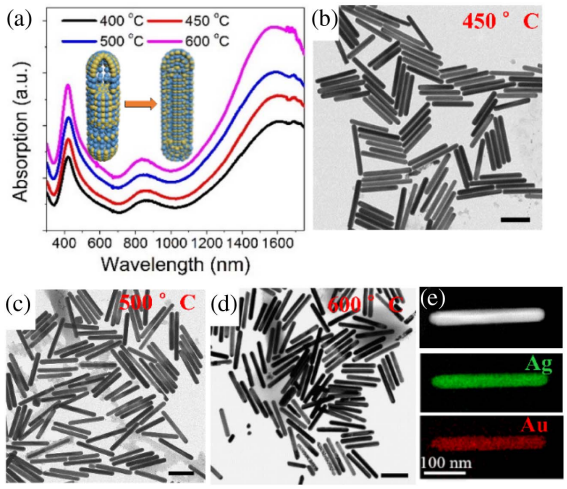

Fig. 3. Annealing temperature effects on alloying of Au and Ag. (a) UV-vis-NIR absorption spectra and (b)–(d) corresponding TEM images of alloyed Au-Ag NRs obtained at annealing temperatures of 450°C, 500°C, and 600°C. The inset of (a) is the evolution schematics of partially and fully alloyed Au-Ag NRs. (e) The elemental distribution of fully alloyed Au-Ag NRs obtained at 450°C (scale bars: 200 nm).

attributed that the SPR_T mode is not capable of characterizing the property of full structure but only that in the surface shell. The TEM images in Figs. 3(b)–3(d) display the change of aspect ratio. Compared with the samples annealed at 400°C, EDX mapping of NRs annealed at 450°C shows homogeneous distributions of Ag and Au elements, indicating the formation of fully alloyed NRs [Fig. 3(e)]. The evolution schematics from partially to fully alloyed NRs are illustrated by the inset in the UV-vis-NIR spectra of Fig. 3. It can be obtained that an alternative approach to fabricate fully alloyed NRs with different aspect ratios is to uniformly anneal SiO_2-coated Au@Ag core-shell NRs based on well-defined Au NBPs at 450°C.

B. Chemical and Thermal Stability

As is well known, chemical and thermal stability are critical for some practical applications. The tests on chemical stability are exhibited by incubating both Au@Ag core-shell NRs and alloyed Au-Ag NRs in etchant solution including NH_4OH and H_2O_2. The spectra and corresponding TEM images in Fig. 4 demonstrate that Au@Ag core-shell NRs will decay to Au NBPs within 15 min since Ag shell is oxidized and etched, and the colloid change from green to brown [inset of Fig. 4(a)]. However, both the spectra and morphology of alloyed NRs in Fig. 4(b) have no obvious transformation. As a consequence, it could be deemed that alloying of Au and Ag can improve the chemical stability of rod-like nanostructures. Interestingly, partially alloyed Au-Ag NRs produce hollow ends, which is attributed to the oxidation of Ag-rich parts in the ends, as shown in Fig. 4. For the fully alloyed samples, no hollow ends can be found after etching, and the morphology of samples is well retained.

In particular, the increased Au weight relative to Ag also would promote the chemical stability of alloyed NRs. Experiments on changing the size of the Au NBPs core of the core-shell precursor are carried out to fabricate different composition ratios (Ag/Au) of alloyed NRs. Figures 4(d)–4(g) illustrate that a small number of hollow ends appear for alloyed NRs with the increasing size of Au NBPs (or the decreasing Ag/Au composition ratio). It can be revealed that partially alloyed Au-Ag NRs with low Au weight present larger hollow ends after etching in NH_4OH and H_2O_2 solution. Therefore, the larger supply of Au atoms facilitates full alloying. As mentioned above, by annealing core-shell NRs with a high Ag/Au composition ratio at 450°C, uniformly alloyed NRs are achieved [inset in Fig. 4(d)]. Consequently, for the case of a precursor with a moderate composition ratio of Ag/Au, fully alloyed NRs possess excellent chemical stability.

To investigate the thermal stability, alloyed Au-Ag NRs annealed at different temperatures were further heated to 600°C in N_2 or air atmosphere. Table 1 summarizes products in different annealing conditions. The corresponding optical spectra and TEM images in Fig. 5 demonstrate that the morphologies of alloyed NRs slightly change, when the products were reannealed in N_2 (samples 1 and 3). It is therefore revealed that re-annealing will induce re-diffusion of Au and Ag atoms. However, annealing partially alloyed NRs at 600°C in air could induce structural deformation, while fully alloyed NRs keep stable. Moreover, Au@Ag@SiO_2 core-shell NRs under one-step annealing in air would transform into alloyed nanoparticles. It further proves that full alloying of Au and Ag would improve structural thermal and chemical stability. For partially alloyed NRs, Ag atoms could sublimate during the process of annealing in air, leading to the appearance of vacancy between the SiO_2-shell and alloyed NR, or even the formation of nanoparticles.

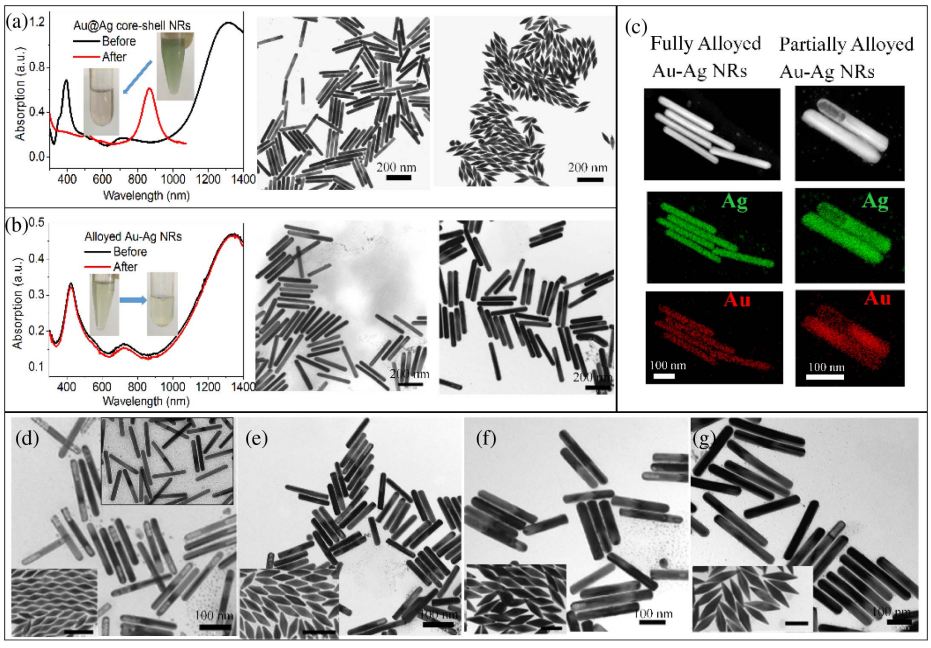

Fig. 4. UV-vis-NIR absorption spectra and corresponding TEM images of (a) Au@Ag core-shell NRs and (b) alloyed Au-Ag NRs before and after incubated in NH_4OH and H_2O_2 solution. The insets in (a),(b) are corresponding colloidal products. The following samples were etched and further observed. (c) HAADF-STEM images and corresponding elemental distribution of fully/partially alloyed Au-Ag NRs. (d)–(g) TEM images of alloyed Au-Ag NRs with increasing Au composition under annealing at 400°C. The bottom insets in (d)–(g) are TEM images of Au NBPs, and the top inset in (d) is the TEM image of alloyed Au-Ag NRs by annealing at 450°C.

Table 1. Morphology Evolution of As-Prepared Alloyed NRs after Re-Annealing at Higher Temperatures in an N_2 or Air Atmosphere[a]

Sample	1	2	3	4	5
T_1 (°C)	400	400	450	450	600
Atmosphere	N_2	N_2	N_2	N_2	Air
Time (min)	10	10	10	10	10
Alloying	Partial	Partial	Full	Full	
T_2 (°C)	600	600	600	600	
Atmosphere	N_2	Air	N_2	Air	
Time (min)	10	10	10	10	
Product	Fully alloyed NRs	Deformation	Fully alloyed NRs	Fully alloyed NRs	Deformation

[a]Wherein, T_1 is the initial annealing temperature, T_2 is the re-annealing temperature, and time is the heat preservation period.

C. SERS Signal Stability

Because of the excellent plasmonic properties, fully alloyed Au-Ag NRs will be ideal candidates for molecule detection based on SERS measurement. SERS spectral stability of R6G-absorbed alloyed NRs and core-shell NRs is investigated. The absorption spectra of samples present the same resonance intensity [Fig. 6(a)]. It can be known from Figs. 6(b) and 6(c) that SERS signals of R6G on alloyed NRs and core-shell NRs are remarkably enhanced (the characteristic peak of R6G is assigned [39]). In general, SERS enhancement of Ag nanostructures should be stronger than that of the same Au-Ag alloy. However, the enhancement intensity of alloyed NRs is higher than that of core-shell NRs, which can be attributed to the oxidation of the Ag shell. This result is also in accordance with the previous report on alloyed nanoparticles [19]. Moreover, when the samples were placed in the etching solution, the SERS signal of alloyed NRs is stable even after 12 h, while that of core-shell NRs is decreasing due to the etching of Ag atoms. Therefore, alloyed Au-Ag NRs will be a stable substrate of SERS enhancement.

D. Drug-Release Improvement

Alloyed Au-Ag NRs coated by mesoporous silica can provide stability storage spaces for small molecules, and thus serve as drug carriers [Fig. 7(a)]. DOX is selected as model guest to be loaded in the alloyed Au-Ag NRs@SiO_2. Notably, the hollow silica capping would be formed due to oxidation of partial Ag atoms when the annealing atmosphere was in air instead of N_2 flow, as shown in Fig. 7(b). It can be proposed that the hollow silica end can provide much more space to store drug molecules, except for dispersing in the mesoporous and absorbing on the surface. Figure 7(c) demonstrates that the loading efficiency of DOX on alloyed NRs with hollow capping (5.4 wt%) is ~2.8 times as high as the full silica capping one (1.93 wt%). The two types of alloyed NRs colloids have the same intensity of SPR_L located at 980 nm, indicating that these samples possess the same particle numbers. The cumulative DOX release profile from alloyed Au-Ag NRs@SiO_2 with or without irradiation of the 980 nm laser is shown in Fig. 7(d). For hollow silica capping, the release can reach the equilibrium state within 5 h. It can be observed that the release of DOX is faster under 980 nm laser irradiation, and the release is 8.5% higher than that without laser irradiation. These are because

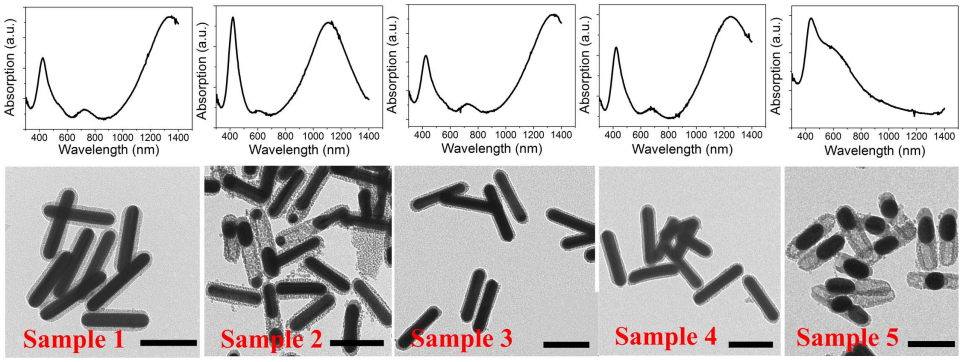

Fig. 5. UV-vis-NIR absorption spectra and corresponding TEM images of as-prepared alloyed NRs after re-annealing at higher temperatures in an N_2 or air atmosphere.

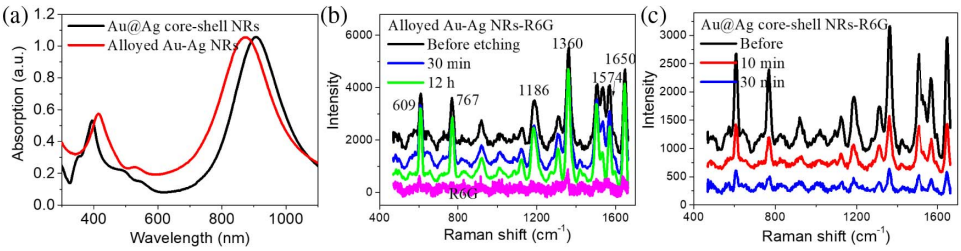

Fig. 6. (a) UV-vis-NIR absorption spectra of core-shell and alloyed NRs with the same resonance intensity. (b), (c) SERS spectra of R6G absorbed on alloyed and core-shell NRs-loaded substrates before and after etching in NH_4OH and H_2O_2.

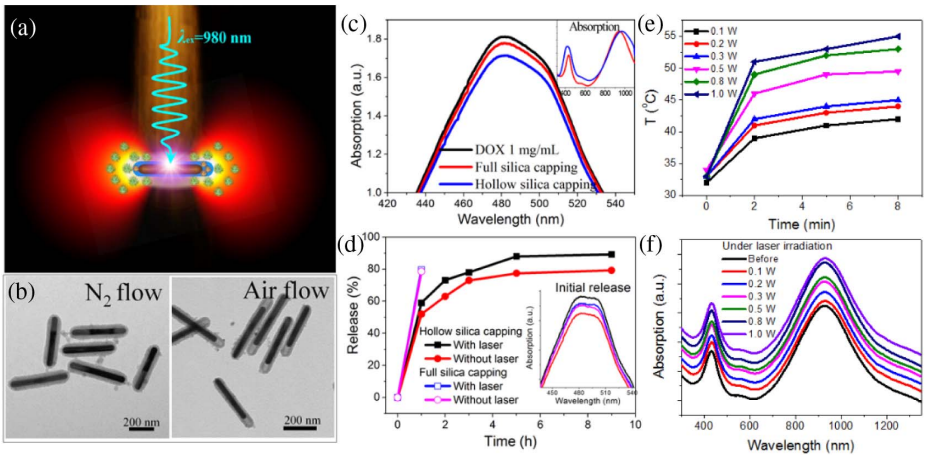

Fig. 7. (a) Schematic of DOX release under 980 nm laser irradiation. (b) TEM images of alloyed Au-Ag NRs with full and hollow silica capping by annealing in N_2 flow and air, respectively. (c) UV-vis-NIR absorption spectra of free DOX molecules before and after being loaded on alloyed Au-Ag NRs. The inset in (c) is the absorption spectra of alloyed Au-Ag NRs coated by full/hollow mesoporous silica. (d) DOX release profiles with and without laser irradiation. The inset in (d) is the absorption spectra of released DOX after 1 h. (e) The photo-thermal conversion and (f) corresponding UV-vis-NIR spectra of alloyed Au-Ag NRs (1 mL) under irradiation of a 980 nm laser with different powers (laser spot: 2 mm × 2 mm).

alloyed NRs with SPR located at the NIR window (~980 nm) have excellent photo-thermal effects under irradiation of 980 nm laser [40,41]. The irradiation leads to the rapid temperature rising of alloyed NRs colloid without morphology evolution [Figs. 7(e) and 7(f)], which facilitates the release of DOX. However, the drugs carried on full silica capping will be quickly released, in which condition the photo-thermal effect can be neglected. Hence, the stable alloyed NRs with hollow silica capping are promising drug carries.

4. CONCLUSION

In summary, alloyed Au-Ag NRs with high aspect ratios have been achieved by annealing Au@Ag core-shell NRs coated by mesoporous silica at 450°C. The alloyed NRs exhibit excellent SPR properties and high stability. Different from the SPR modes of monometallic NRs, both the SPR_L (600–1800 nm) and SPR_T (400–500 nm) modes of alloyed NRs can be tuned. SPR peaks can shift in a large wavelength region by adjusting the aspect ratio and composition ratio. Under annealing at the critical temperature of phase transition, alloying of Au and Ag for a high aspect ratio of NRs prefers to form partially alloyed Au-Ag NRs. With an increase in the annealing temperature, the atomic diffusivity is intensified, resulting in the transformation from partially to fully alloyed NRs. Alloying of Au@Ag core-shell NRs with a moderate composition ratio of Ag/Au can remarkably improve the chemical stability of NRs, although hollow ends can be generated for this case. Meanwhile, the fully alloyed NRs also possess high thermal stability. The morphology has no obvious deformation under annealing temperatures as high as 600°C in air, while core-shell NRs would turn into nanoparticles. Based on the tunable SPR properties and excellent (chemical and thermal) stability, alloyed Au-Ag NRs can serve as the substrate of SERS enhancement. More sensitive and stable SERS signal enhancement of R6G from the alloyed Au-Ag NRs substrate can be detected compared with Au@Ag core-shell NRs. Additionally, fully alloyed NRs with hollow silica capping can be used to store and release the drug. The release efficiency will be higher due to the high temperature triggered by the photo-thermal effect. As a consequence, it is expected that well-defined alloyed NRs with tunable plasmonic properties and high stability can extend to the applications of bio-medical and other related fields.

Funding. National Natural Science Foundation of China (NSFC) (11774050, 11774171, 11874220, 51571060); National Key R&D Program of China (2017YFA0305500); Open Fund of Key Laboratory for Intelligent Nano Materials and Devices of the Ministry of Education (INMD-2016M05).

Acknowledgment. The authors thank Xiaoguang Zhu from the Institute of Solid State Physics at the Chinese Academy of Sciences for help with the EDX measurements. The authors declare that there are no conflicts of interest related to this article.

REFERENCES

1. R. W. Yu, L. M. Liz-Marzán, and F. J. G. de Abajo, "Universal analytical modeling of plasmonic nanoparticles," Chem. Soc. Rev. **46**, 6710–6724 (2017).
2. A. W. Schell, A. Kuhlicke, G. Kewes, and O. Benson, "'Flying plasmons': Fabry-Pérot resonances in levitated silver nanowires," ACS Photon. **4**, 2719–2725 (2017).
3. J. X. Zhang and L. D. Zhang, "Nanostructures for surface plasmons," Adv. Opt. Photon. **4**, 157–321 (2012).
4. H. C. Chen, C. Y. Cheng, H. C. Lin, H. H. Chen, C. H. Chen, C. P. Yang, K. H. Yang, C. M. Lin, T. Y. Lin, C. M. Shih, and Y. C. Liu, "Multifunctions of excited gold nanoparticles decorated artificial kidney with efficient hemodialysis and therapeutic potential," ACS Appl. Mater. Interfaces **8**, 19691–19700 (2016).
5. C. Y. Li, M. Meng, S. C. Huang, L. Li, S. R. Huang, S. Chen, L. Y. Meng, R. Panneerselvam, S. J. Zhang, B. Ren, Z. L. Yang, J. F. Li, and Z. Q. Tian, "'Smart' Ag nanostructures for plasmon-enhanced spectroscopies," J. Am. Chem. Soc. **137**, 13784–13787 (2015).
6. H. Y. Chen, Y. F. Di, D. Chen, K. Madrid, M. Zhang, C. P. Tian, L. P. Tang, and Y. Q. Gu, "Combined chemo- and photo-thermal therapy delivered by multifunctional theranostic gold nanorod-loaded microcapsules," Nanoscale **7**, 8884–8897 (2015).

7. W. B. Hou and S. B. Cronin, "A review of surface plasmon resonance-enhanced photocatalysis," Adv. Funct. Mater. **23**, 1612–1619 (2013).
8. D. S. Wang and Y. D. Li, "Bimetallic nanocrystals: liquid-phase synthesis and catalytic applications," Adv. Mater. **23**, 1044–1060 (2011).
9. H. Y. Xu, C. X. Kan, C. Z. Miao, C. S. Wang, J. J. Wei, Y. Ni, B. B. Lu, and D. N. Shi, "Synthesis of high-purity silver nanorods with tunable plasmonic properties and sensor behavior," Photon. Res. **5**, 27–32 (2017).
10. N. D. Burrows, S. Harvey, F. A. Idesis, and C. J. Murphy, "Understanding the seed-mediated growth of gold nanorods through a fractional factorial design of experiments," Langmuir **33**, 1891–1907 (2017).
11. N. R. Jana, L. Gearheart, and C. J. Murphy, "Wet chemical synthesis of silver nanorods and nanowires of controllable aspect ratio," Chem. Commun. **2001**, 617–618 (2001).
12. J. S. Liu, C. X. Kan, Y. L. Li, H. Y. Xu, Y. Ni, and D. N. Shi, "End-to-end and side-by-side assemblies of gold nanorods induced by dithiol poly(ethylene glycol)," Appl. Phys. Lett. **104**, 253105 (2014).
13. X. H. Huang, S. Neretina, and M. A. El-Sayed, "Gold nanorods: from synthesis and properties to biological and biomedical applications," Adv. Mater. **21**, 4880–4910 (2009).
14. C. X. Kan, C. S. Wang, H. C. Li, J. S. Qi, J. J. Zhu, and Z. S. Li, "Gold microplates with well-defined shapes," Small **6**, 1768–1775 (2010).
15. X. Z. Zhu, X. L. Zhuo, Q. Li, Z. Yang, and J. F. Wang, "Gold nanobipyramid-supported silver nanostructures with narrow plasmon linewidths and improved chemical stability," Adv. Funct. Mater. **26**, 341–352 (2016).
16. B. Wiley, Y. G. Sun, and Y. N. Xia, "Synthesis of silver nanostructures with controlled shapes and properties," Acc. Chem. Res. **40**, 1067–1076 (2007).
17. D. Rioux, S. Vallières, S. Besner, P. Munoz, E. Mazur, and M. Meunier, "An analytic model for the dielectric function of Au, Ag, and their alloys," Adv. Opt. Mater. **2**, 176–182 (2014).
18. Y. Y. Wu, G. L. Li, C. Cherqui, N. W. Bigelow, N. Thakkar, D. J. Masiello, J. P. Camden, and P. D. Rack, "Electron energy loss spectroscopy study of the full plasmonic spectrum of self-assembled Au-Ag alloy nanoparticles: unraveling size, composition, and substrate effects," ACS Photon. **3**, 130–138 (2016).
19. Y. M. Si, Y. C. Bai, X. J. Qin, J. Li, W. W. Zhong, Z. J. Xiao, J. S. Li, and Y. D. Yin, "Alkyne-DNA-functionalized alloyed Au/Ag nanospheres for ratiometric surface-enhanced Raman scattering imaging assay of endonuclease activity in live cells," Anal. Chem. **90**, 3898–3905 (2018).
20. Y. H. Cheng, Y. Zhang, S. L. Chau, S. K. M. Lai, H. W. Tang, and K. M. Ng, "Enhancement of image contrast, stability, and SALDI-MS detection sensitivity for latent fingerprint analysis by tuning the composition of silver-gold nanoalloys," ACS Appl. Mater. Interfaces **8**, 29668–29675 (2016).
21. A. Hatef, B. Darvish, A. Dagallier, Y. R. Davletshin, W. Johnston, J. C. Kumaradas, D. Rioux, and M. Meunier, "Analysis of photoacoustic response from gold-silver alloy nanoparticles irradiated by short pulsed laser in water," J. Phys. Chem. C **119**, 24075–24080 (2015).
22. R. Rajendra, P. Bhatia, A. Justin, S. Sharma, and N. Ballav, "Homogeneously-alloyed gold-silver nanoparticles as per feeding moles," J. Phys. Chem. C **119**, 5604–5613 (2015).
23. I. Lee, S. W. Han, and K. Kim, "Production of Au-Ag alloy nanoparticles by laser ablation of bulk alloys," Chem. Commun. **2001**, 1782–1783 (2001).
24. C. Wang, S. Peng, R. Chan, and S. H. Sun, "Synthesis of AuAg alloy nanoparticles from core/shell-structured Ag/Au," Small **5**, 567–570 (2009).
25. C. Wang, H. G. Yin, R. Chan, S. Peng, S. Dai, and S. H. Sun, "One-pot synthesis of oleylamine coated AuAg alloy NPs and their catalysis for CO oxidation," Chem. Mater. **21**, 433–435 (2009).
26. Y. G. Sun and Y. N. Xia, "Alloying and dealloying processes involved in the preparation of metal nanoshells through a galvanic replacement reaction," Nano Lett. **3**, 1569–1572 (2003).
27. Q. B. Zhang, J. Y. Lee, J. Yang, C. Boothroyd, and J. X. Zhang, "Size and composition tunable Ag-Au alloy nanoparticles by replacement reactions," Nanotechnology **18**, 245605 (2007).
28. X. Y. Wei, Q. K. Fan, H. P. Liu, Y. C. Bai, L. Zhang, H. Q. Zheng, Y. D. Yin, and C. B. Gao, "Holey Au-Ag alloy nanoplates with built-in hotspots for surface-enhanced Raman scattering," Nanoscale **8**, 15689–15695 (2016).
29. C. B. Gao, Y. X. Hu, M. S. Wang, M. F. Chi, and Y. D. Yin, "Fully alloyed Ag/Au nanospheres: combining the plasmonic property of Ag with the stability of Au," J. Am. Chem. Soc. **136**, 7474–7479 (2014).
30. T. Zhang, F. Zhou, L. F. Hang, Y. Q. Sun, D. L. Liu, H. L. Li, G. Q. Liu, X. J. Lyu, C. C. Li, W. P. Cai, and Y. Li, "Controlled synthesis of sponge-like porous Au-Ag alloy nanocubes for surface-enhanced Raman scattering properties," J. Mater. Chem. C **5**, 11039–11045 (2017).
31. J. F. Huang, Y. H. Zhu, C. X. Liu, Y. F. Zhao, Z. H. Liu, M. N. Hedhili, A. Fratalocchi, and Y. Han, "Fabricating a homogeneously alloyed AuAg shell on Au nanorods to achieve strong, stable, and tunable surface plasmon resonances," Small **11**, 5214–5221 (2015).
32. W. H. Qi and S. T. Lee, "Phase stability, melting, and alloy formation of Au-Ag bimetallic nanoparticles," J. Phys. Chem. C **114**, 9580–9587 (2010).
33. W. Albrecht, J. E. S. van der Hoeven, T. S. Deng, P. E. de Jongh, and A. van Blaaderen, "Fully alloyed metal nanorods with highly tunable properties," Nanoscale **9**, 2845–2851 (2017).
34. Y. C. Bai, C. B. Gao, and Y. D. Yin, "Fully alloyed Ag/Au nanorods with tunable surface plasmon resonance and high chemical stability," Nanoscale **9**, 14875–14880 (2017).
35. A. Sánchez-Iglesias, N. Winckelmans, T. Altantzis, S. Bals, M. Grzelczak, and L. M. Liz-Marzán, "High-yield seeded growth of monodisperse pentatwinned gold nanoparticles through thermally induced seed twinning," J. Am. Chem. Soc. **139**, 107–110 (2017).
36. Q. Li, X. L. Zhuo, S. Li, Q. F. Ruan, Q. H. Xu, and J. F. Wang, "Production of monodisperse gold nanobipyramids with number percentages approaching 100% and evaluation of their plasmonic properties," Adv. Opt. Mater. **3**, 801–812 (2015).
37. J. J. Wei, C. X. Kan, Y. K. Lou, Y. Ni, H. Y. Xu, and C. S. Wang, "Synthesis and stability of bimetallic Au@Ag nanorods," Superlattice. Microst. **100**, 315–323 (2016).
38. X. Z. Zhu, H. K. Yip, X. L. Zhuo, R. B. Jiang, J. L. Chen, X. M. Zhu, Z. Yang, and J. F. Wang, "Realization of red plasmon shifts up to ~900 nm by AgPd-tipping elongated Au nanocrystals," J. Am. Chem. Soc. **139**, 13837–13846 (2017).
39. W. Y. Tao, A. W. Zhao, H. H. Sun, Z. B. Gan, M. F. Zhang, D. Li, and H. Y. Guo, "Periodic silver nanodishes as sensitive and reproducible surface-enhanced Raman scattering substrates," RSC Adv. **4**, 3487–3493 (2014).
40. A. M. Smith, M. C. Mancini, and S. M. Nie, "Bioimaging: second window for *in vivo* imaging," Nat. Nanotechnol. **4**, 710–711 (2009).
41. Y. Qiao, F. Ma, C. Liu, B. Zhou, Q. L. Wei, W. L. Li, D. N. Zhong, Y. Y. Li, and M. Zhou, "Near-infrared laser-excited nanoparticles to eradicate multidrug-resistant bacteria and promote wound healing," ACS Appl. Mater. Interfaces **10**, 193–206 (2018).